Journal of Oceanology and Limnology
Vol. 44, No. 2, pp. 492-510, 2026
https://doi.org/10.1007/s00343-025-5015-2

Research Paper

Zonal asymmetry of recent heat content change in Antarctic Intermediate Water*

Xubin NI[1, 2], Ling DU[1, 2, **], Linlin FAN[1, 2], Huangyuan SHI[3]

[1] *Frontier Science Center for Deep Ocean Multispheres and Earth System (FDOMES) and Physical Oceanography Laboratory, Ocean University of China, Qingdao 266100, China*
[2] *College of Oceanic and Atmospheric Sciences, Ocean University of China, Qingdao 266100, China*
[3] *College of Ocean and Meteorology, Guangdong Ocean University, Zhanjiang 524000, China*

Received Jan. 16, 2025; accepted in principle Apr. 30, 2025; accepted for publication Jun. 16, 2025

Abstract Climate changes lead to significant warming of the Southern Ocean. By analyzing observational products and objective analysis data, this study reveals that the Antarctic Intermediate Water (AAIW) shows a zonal asymmetry of heat content changes, resulting from the different regional responses to the large-scale circulations. The heat content changes show significant interannual to decadal variations superimposed on a long-term trend, mainly attributed to the heat redistribution affected by the atmospheric circulations. AAIW in the Indian sector exhibits a significant widespread warming, and AAIW in the southwest Pacific sector presents an unexpected cooling. Warming has increased by 0.4 ZJ (zettajoules, 1 ZJ=10^{21} J) per decade since 1979 in the Indian sector, which is equivalent to the heat gain rate of 0.04 W/m^2 during 1979–2019 in the Southern Ocean. Upwelling of warm circumpolar deep water driven by upward Ekman pumping, induced by the persistent positive phase of the Southern Annular Mode in recent years, plays a leading role in promoting this warming. The unexpected cooling in the southwest Pacific sector, reaching -0.2 ZJ per decade during 1979–2019, is due to the increasing cold water from sea ice and melting water. An increase of low-pressure anomaly facilitates the shallowing and tilting of isopycnals and the intrusion of cold water into the interior ocean, which is closely associated with the Atlantic multidecadal oscillation. The enhancement of this zonal asymmetry in the AAIW shows an increasing heat content in the Indian sector and a decreasing heat content in the Pacific sector, which implies that the Indian Ocean will become an important potential warming pool in the future.

Keyword: Antarctic Intermediate Water (AAIW); Southern Ocean; climate variability; zonal asymmetry

1 INTRODUCTION

The Southern Ocean has been warming significantly in response to global warming (Sallée, 2018), as the studies recording the remarkable increase of the ocean heat content (OHC) above 2 000 m (Kolodziejczyk et al., 2019; Carter et al., 2022). The Southern Ocean has absorbed substantial anthropogenic heat near 60°S induced by the poleward-intensified wind changes (Liu et al., 2018). This conspicuous warming emphasizes that there is outstanding warming in the prominent water masses in the Southern Ocean, such as the Antarctic Intermediate Water (AAIW) (Dufour et al., 2015; Gao et al., 2018). The intermediate water mass, as a key branch of the upper overturning circulation, plays a vital role in Earth's climate system by contributing to the northward return flow from the Southern Ocean to the northern hemisphere (Schmitz and McCartney, 1993; Abernathey et al., 2016).

AAIW has the salinity minimum and can be identified by the potential density range of 27.2–27.5 kg/m^3, and the salinity range of 34.2–34.5

* Supported by the National Natural Science Foundation of China (Nos. 42230405, 42376256, 41576020) and the National Key Research and Development Program of China (No. 2018YFA0605701)
** Corresponding author: duling@ouc.edu.cn

(Carter et al., 2008; Portela et al., 2020; Li et al., 2022). The latest research by Zhou et al. (2024) used volumetric maxima and minima potential density range between 27.1 and 27.4 kg/m^3 to analyze AAIW. In the south of the Subantarctic Front (SAF), the ventilated AAIW is mainly generated by the polar ocean's cold and fresh Antarctic Surface Water (Downes et al., 2017; Carter et al., 2022; Li et al., 2022), while in the north of the SAF, AAIW is closely associated with the overlaying Subantarctic Mode water (SAMW). SAMW is identified by the minimum of potential vorticity, and partly supplies the AAIW by mixing (Li et al., 2022). Heat content and properties of AAIW have also experienced significant changes after the 1980s, including the distinct features of the temperature/salinity fields. The most significant warming trend of AAIW occurs in the south Indian Ocean (Dufour et al., 2015), while AAIW in the south Pacific shows a cooling trend after 2006 (Kolodziejczyk et al., 2019). On changes in salinity, AAIW is freshening significantly since the 1980s–1990s (Carter et al., 2022), and this freshening continues in the 21st century (Schmidtko and Johnson, 2012). AAIW also exhibits the salinification around the south of Australia and Africa (Marshall et al., 2013). Temperature is closely related to heat content, as warming/cooling of water mass also reflects in the increase/decrease of heat content. On the other hand, the changes of temperature and salinity cause the changes of density, and the isopycnal shallows or deepens to maintain the same density. Thus, the thickness of the water masses between the different isopycnals changes. The thickness also plays a key role in heat content changes of AAIW (Portela et al., 2020).

The significant changes of AAIW occur in mainly the high-latitude south of SAF, which is closely related to the changes of wind field and sea ice formation/export, which are affected by the large-scale circulation (Meijers et al., 2011; Downes et al., 2017). Previous studies show that the different large-scale circulations have distinct impacts on the South Indian Ocean and the South Pacific Ocean (Nuncio and Yuan, 2015; Li et al., 2021). The South Indian Ocean is mainly affected by the Southern Annular Mode (SAM) and Indian Ocean Dipole (IOD). SAM is one of the most important atmospheric variability to modulate the Southern Hemisphere (SH) climate and is characterized by a strong circumpolar westerly wind (Jones et al., 2019). The frequent positive phase of SAM has occurred since 1979, resulting in an increase of westerly winds around 60°S, especially in the south Indian Ocean (50°S–62°S, 60°E–140°E) (Marshall et al., 2013). This enhanced zonal wind brings about increasing northward transport of surface fresh and cold water, and then affects the temperature/salinity changes of AAIW. And IOD affects the increase/decrease of sea ice formation and subsequent change of sea surface temperature (Nuncio and Yuan, 2015). On the other hand, the South Pacific Ocean is affected significantly by Interdecadal Pacific Oscillation (IPO) and Atlantic Multidecadal Oscillation (AMO), leading to that temperature changes are significant on the interdecadal timescale (Li et al., 2021; Song et al., 2024). IPO and AMO enhance the low-pressure system via the teleconnection, which is derived from the sea surface temperature (SST) anomalies of the tropical Pacific and Atlantic, and then Rossby waves propagate to the south Pacific Ocean (Li et al., 2015). IPO and AMO have both experienced the obvious transition of phases since the 1980s. These transitions cause the changes of the strength of the low-pressure system via the Ekman transports and Ekman pumping, resulting in heat convergence/divergence and sea ice production (Gao et al., 2018; Clem et al., 2019; Wang et al., 2021; Song et al., 2024). Additionally, the strength of the low-pressure system is also affected by the zonal wave three, leading to a temperature change of surface water (Chung et al., 2022). This low-pressure system affects sea ice expansion and surface temperature change through meridional wind change (Chung et al., 2022; Kang et al., 2023), and has the most important influence in the South Pacific (52°S–66°S, 130°W–170°W) where significant meridional wind occurs. Hence, how the large-scale circulations affect the heat content and properties of AAIW still requires exploration.

The previous studies show that the heat content and properties of AAIW exhibit a distinction in response to different large-scale circulations, which is mainly attributed to the influence of wind change (Nuncio and Yuan, 2015; Li et al., 2021). Therefore, by using the observationally based products and objective analysis data, we explored the temporal and spatial variation of heat content in AAIW, and found that the recent heat content trend of AAIW show a zonal asymmetry between the South Indian Ocean and the South Pacific Ocean. This zonal asymmetry is significant on the interdecadal timescale, which is modulated by the complicated

large-scale circulations. We also analyzed the mechanism of this zonal asymmetry of heat content change on the interannual to decadal timescales, and explained the influence of wind modulated by the large-scale circulation. The paper is organized as follows: Section 2 describes the datasets and methods. Section 3.1 investigates the recent heat content changes of AAIW associated with atmospheric circulations. Sections 3.2 and 3.3 include the effect and detailed processes on different timescales. Section 4 provides a summary and further discussion.

2 DATA AND METHOD

The analysis of AAIW is mainly based on the ocean temperature/salinity objectively analyzed data, Ishii 7.3 (Ishii et al., 2017). The Ishii data are based on the Argo Project, World Ocean Data 2013, and the Global Temperature-Salinity Profile Program. The global ocean heat content estimated by Ishii showed good consistency with other observations and thus, Ishii has been adopted in both the Fifth and Sixth Assessment Report of the Intergovernmental Panel on Climate Change to estimate climate change. It has 1°×1° horizontal resolution and 28 levels from 1955 to 2019, and the heat content anomalies calculated by Ishii are consistent with the Levitus09 in the Southern Ocean. The period from 1979 to 2019 is used in this study.

The temperature/salinity observations used in this study include World Ocean Database 2018 (WOD 18), World Ocean Atlas 2018 (WOA 18), and Grid Point Value of the Monthly Objective Analysis using the Argo data (as MOAA GPV and hereinafter). The quality-controlled temperature/salinity profiles dataset, WOD 18, is provided by the National Centers for Environmental Information (NCEI), the National Oceanic and Atmospheric Administration (NOAA), USA. Sampling of WOD 18 includes ships, floats, and conductivity-temperature-depth, and so on (Boyer et al., 2018), and has an average of ~365 temperature/salinity profiles for every 10 longitudes from 1979 to 2019 (Fig.1e) in the south of 40°S. WOD 18 has 3 549 profiles in the Indian sector and 709 profiles in the southwest Pacific sector. These profiles are equivalent to about one profile per one grid point in each sector. The gridded temperature/salinity observation, WOA, has climatological fields with an interval of 10 years (Locarnini et al., 2019; Zweng et al., 2019). The temperature/salinity fields in 1975–1984, 1985–1994, 1995–2004, and 2005–2017 are used in this study. Another gridded observation dataset, MOAA GPV, is provided by the Japan Agency for Marine-Earth Science and Technology. The temperature/salinity of MOAA GPV uses the data from Argo floats, the Triangle Trans-Ocean Buoy Network, and available conductivity-temperature-depth casts. It contains optimally interpolated temperature and salinity values at selected standard pressure levels on a 1° grid in the global ocean (Hosoda, 2007).

The monthly sea ice concentration (SIC) fields used in this study, Climate Data Record of Passive Microwave Sea Ice Concentration Version 3, is provided by the American National Snow & Ice Data Center (Comiso and Nishio, 2008). We utilized the 500-hPa geopotential height and 10-m wind field from the fifth generation ECMWF atmospheric reanalysis (ERA5), produced by the European Centre for Medium-Range Weather Forecasts (ECMWF) Integrated Forecast System. ERA5 is freely available from the Copernicus Climate Change Service in Climate Data Store (Hersbach et al., 2019a, b). ERA5 has combined model data with observations and provided many types of atmospheric variables with a longer term from 1979, and then has taken the place of ERA-Interim reanalysis. The horizontal resolution of monthly datasets is 0.25°×0.25°. The sea surface net heat flux data from the Ocean Reanalysis System 5 (ORAS5) is also used in this study to analyze the heat content change in AAIW. ORAS5 is provided by ECMWF and freely available in the Climate Data Store.

Figure 1 shows the temperature and salinity of the Ishii data and WOD 18. The mean temperature/salinity profiles of WOD 18 are the average of all samplings in the region from 1979 to 2019. And the mean temperature/salinity profiles of the Ishii data are the average of all profiles over the overlapping period of WOD 18 (Fig.1a–d). Salinity derived from Ishii data and WOD 18 shows consistency in 0–2 000 m. Temperature in WOD 18 above ~200 m exhibits <0.6 °C colder than this in Ishii data, resulting from those observed samplings in austral autumn mainly (not shown) and affected by the production of sea ice and cold air temperature within the mixed layer (ML). Table 1 shows details that the temperature of the Ishii data shows a general consistency with the observation in 0–1 500 m. The relative ratio of temperature and

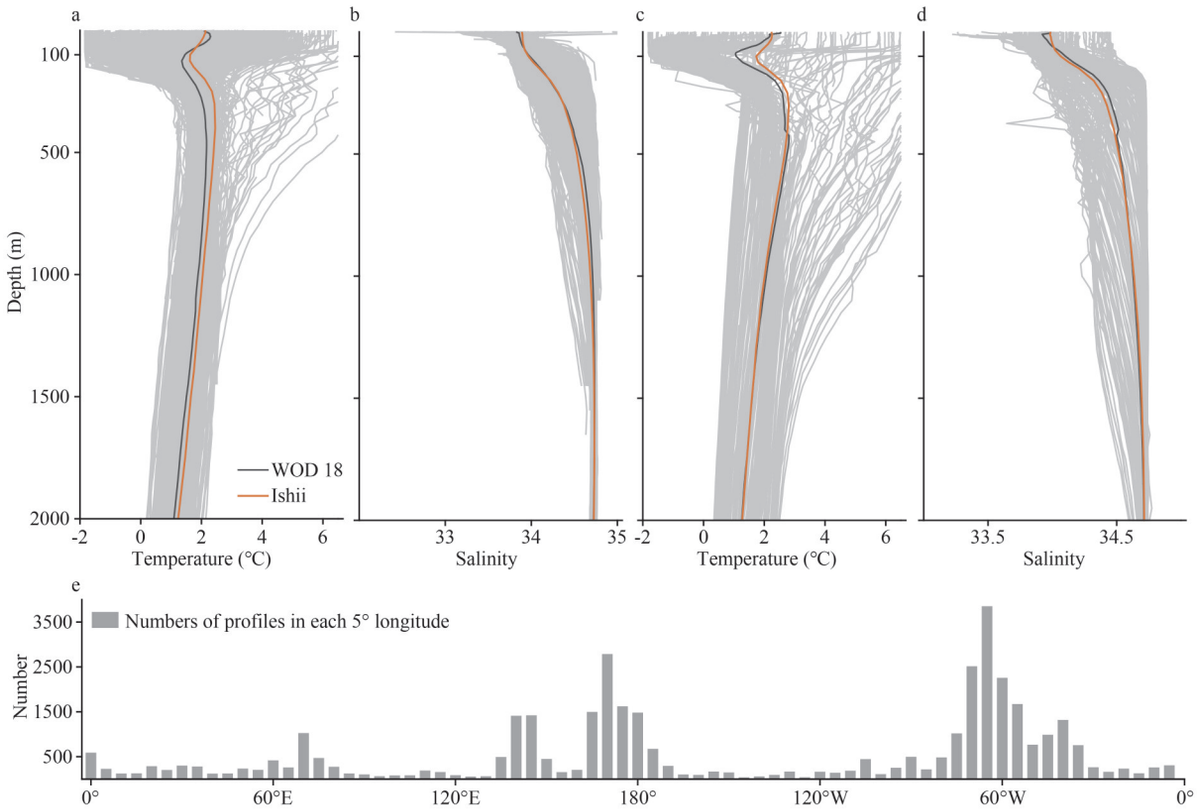

Fig.1 Profiles of temperature and salinity derived from WOD 18 and Ishii in each sector from 1979 to 2019

a. temperature profiles in the Indian sector (as "Ind" hereinafter, 50°S–62°S, 60°E–140°E). The gray line denotes the WOD 18 profiles, and the black line represents the corresponding regional mean temperature profile. The orange line denotes the regional mean temperature profile derived from Ishii; b. same as (a), but is a salinity profile; c and d. same to (a) and (b), respectively but in the southwest Pacific sector (as "Pac" hereinafter, 52°S–66°S, 130°W–170°W); e. distribution of WOD 18 profiles from 1979 to 2019.

Table 1 Mean temperature and salinity of Ishii data and WOD 18

Depth (m)	Indian sector (50°S–62°S, 60°E–140°E)				Pacific sector (52°S–66°S, 130°W–170°W)			
	Diff.[1] T (°C)	Error[2]	Diff.[1] S	Error[2]	Diff.[1] T (°C)	Error[2]	Diff.[1] S	Error[2]
0<depth≤50	-0.17	-0.08	0.03	0.001	0.14	0.07	0.04	0.001
50<depth≤100	-0.02	-0.01	0.01	0.001	0.55	0.43	-0.01	0.001
100<depth≤200	0.34	0.22	-0.02	-0.001	0.29	0.16	-0.05	-0.002
200<depth≤500	0.34	0.16	-0.01	0.001	0.08	0.03	-0.03	-0.001
500<depth≤1 000	0.14	0.07	-0.02	-0.001	-0.11	-0.05	0.00	0.001
1 000<depth≤1 500	0.11	0.06	-0.01	0.001	-0.05	-0.03	0.00	0.001
50<depth≤200	0.11	0.07	0.06	0.001	0.57	0.40	0.04	0.001
50<depth≤1 500	0.10	0.05	0.14	0.004	0.15	0.07	0.07	0.002

1: difference of temperature/salinity between WOD 18 and Ishii, e.g., the difference of temperature (50<depth≤100) is calculated as $\mathrm{Diff.}T=\overline{\int_{50}^{100}T_{\mathrm{Ishii}}\mathrm{d}z}-\overline{\int_{50}^{100}T_{\mathrm{WOA18}}\mathrm{d}z}$; 2: relative ratio of difference, e.g., the relative ratio of temperature (50<depth≤100) is calculated as. $\mathrm{Error.}T=\left(\overline{\int_{50}^{100}T_{\mathrm{Ishii}}\mathrm{d}z}-\overline{\int_{50}^{100}T_{\mathrm{WOA18}}\mathrm{d}z}\right)/\overline{\int_{50}^{100}T_{\mathrm{WOA18}}\mathrm{d}z}$.

salinity above 1 500 m is less than 0.1. The temporal and spatial distribution of OHC changes derived from Ishii is also generally consistent with that from WOA and MOAA GPV (Fig.2a–d).

The calculation of the heat content of AAIW follows the method of Kolodziejczyk et al. (2019). Potential density, neutral density, and salinity minimum, etc., are usually used to define the

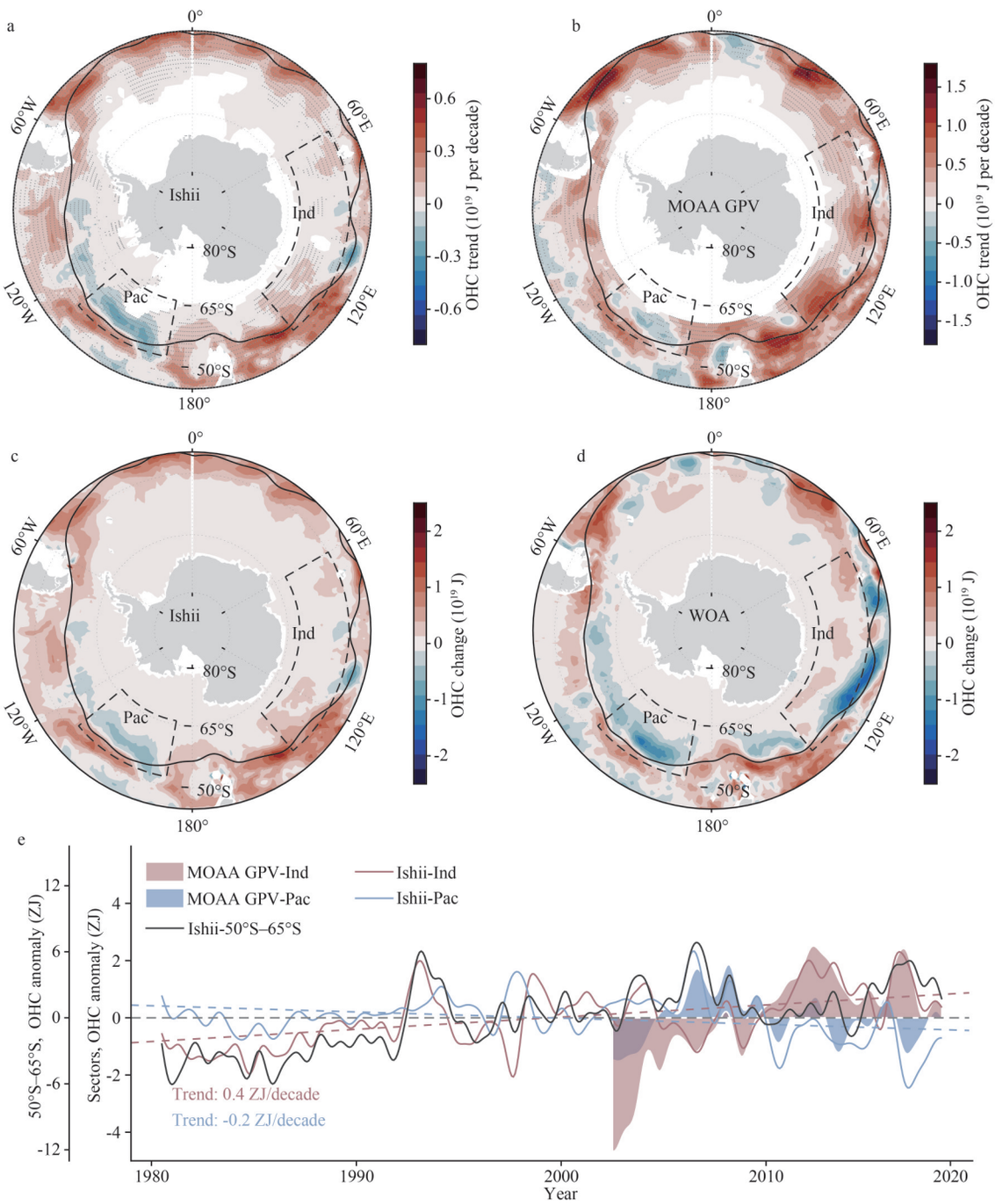

Fig.2 Temporal and spatial variation of heat content in AAIW

a. Ishii, trend during 1979–2019; b. MOAA GPV, trend during 2001–2019; c. Ishii, change of 2005–2019 relative to 1979–1993; d. WOA, change of 2005–2017 relative to 1975–1994. The black line denotes the observed south Subantarctic Front. Dashed black frames present Indian sector (as "Ind" in figure hereinafter, 50°S–62°S, 60°E–140°E), southwest Pacific sector (as "Pac" in figure hereinafter, 52°S–66°S, 130°W–170°W); e. change of regional mean heat content in the Indian and southwest Pacific sectors derived from Ishii (solid lines) and MOAA GPV (shadows). Red (blue) dashed line denotes the linear trend of Ishii during 1979–2019. The black line indicates the change of AAIW heat content in general between 50°S–65°S.

position of AAIW in previous studies (McCartney, 1977; Cerovečki et al., 2019; Portela et al., 2020; Li et al., 2022). Here, considering the density range and salinity minimum below the potential vorticity of SAMW, the potential density range of 27.2– 27.5 kg/m^3 is applied to the AAIW in the Southern Ocean. The AAIW within 27.2–27.5-kg/m^3 potential density shows a general consistency with AAIW identified by neutral density range. The ocean heat content of AAIW is calculated as

followed:

$$\mathrm{OHC}=\int_{27.2\ \mathrm{kg/m^3}}^{27.5\ \mathrm{kg/m^3}}\rho C_p T(z)\,\mathrm{d}z, \quad (1)$$

where the ρ is the seawater density and C_p is the isobaric thermal capacity of the seawater, T is the potential temperature anomaly.

Here, we also check the influence of the range of potential density on heat content change in AAIW. Range of potential density changes from the upper layer of 27.1 kg/m^3 and the lower layer of 27.4 kg/m^3 to the upper layer of 27.2 kg/m^3 and the lower layer of 27.5 kg/m^3, which has little influence on the general distribution of AAIW. The range of potential density changes by 0.1 kg/m^3 only affects <1% changes of AAIW heat content. This little influence can be attributed to that although the surface ocean warms/cools significantly, the thickness between shallow isopycnals in the surface layer is still thin. Although the thickness of deep isopycnals in the deep ocean is relatively thick, the temperature changes are small. Therefore, given the density range of AAIW in different oceans and reducing the influence from SAMW, the potential density range of AAIW within 27.2–27.5 kg/m^3 is used in this study.

3 ZONAL ASYMMETRY OF HEAT CONTENT TREND IN AAIW

Figure 2 displays the heat content of AAIW derived from observations and the Ishii data, and exhibits the trends and changes of heat content during different periods. AAIW has shown a widespread warming since 1979 in the Southern Ocean (Fig.2a & e), as mentioned by Schmidtko and Johnson (2012). In the present study, the most significant warming occurs in the southeast Indian sector and the south Atlantic sector. In particular, in the Indian sector (50°S–62°S, 60°E–140°E) where there is intensified westerly wind (Marshall et al., 2013), warming of AAIW has reached a trend of 0.4 ZJ (zettajoules) per decade (1 ZJ=10^{21} J; Fig.2e; at 95% significant level, derived from Ishii data). However, there is an unexpected cooling event in the southwest Pacific sector, reaching -0.2×10^{19} J per decade. The most significant cooling is persistent, especially between 130°W and 170°W, where there is a significant south wind driven by the low-pressure system (Li et al., 2015). Observation also demonstrates that this cooling trend (-0.5×10^{19} J per decade at 95% significant level) in the southwest Pacific sector also exists during 2001–2019 (Fig.2b). The heat content of AAIW exhibits a decrease of 1×10^{19} J after 2005 compared to pre-1993 (Fig.2c), consisting with the decrease of 2×10^{19} J in the WOA (Fig.2d). The result shows that the general significant warming occupies the Indian sector (50°S–62°S, 60°E–140°E) and the significant cooling occurs in the southwest Pacific sector (52°S–66°S, 130°W–170°W), leading to a zonal asymmetry of the AAIW heat content trend. A similar zonal asymmetry of temperature trend between Indian and southwest Pacific sectors within the Ekman layer is also mentioned in Song et al. (2024). The primary potential density range of AAIW in our study includes partly Antarctic Surface water (AASW). More importantly, our study finds that an unexpected zonal asymmetry existed in the intermediate ocean rather than limited to the surface layer. We further reveal that the zonal asymmetry becomes statistically significant after 2005. The correlation coefficients of heat content in AAIW between the Indian sector and the Pacific sector changed from 0.47 (1979–1993) to -0.69 (2005–2019), and the correlation coefficient reaches -0.45 during 1979–2019 (not shown) (at 95% significance level). The enhancement of the zonal asymmetry of heat content change in AAIW is closely associated with the different influence of wind (more details in Section 4).

The zonal mean temperature trend of the AAIW between the Indian Ocean and the southwest Pacific sector also shows an obvious zonal asymmetry (Fig.3). In the Indian Ocean sector, warming is significant near the surface, and the warming trend weakens with depth (Fig.3a). The most significant warming mainly occurs between the density range of 27.2–27.6 kg/m^3, where there is mostly the AAIW. Specifically, the AAIW in the south of 60°S is obducted and is warming significantly over 400 m. The strongest warming trend is more than 0.2 °C per decade. It can be seen that the increase of heat content in the Indian Ocean sector is significantly related to the surface warming, which may be related to the increase of heat gain in the Southern Ocean after 2005 (Kolodziejczyk et al., 2019). However, AAIW in the southwest Pacific sector showed an unexpected cooling (Fig.3b). The strongest cooling is found between 27.2–27.6 kg/m^3, mainly the AAIW. AAIW in the south of 55°S has a significant cooling with a trend of -0.2 °C per decade, reaching a depth of 1 000 m. This cooling is also most significant near the surface, and like a

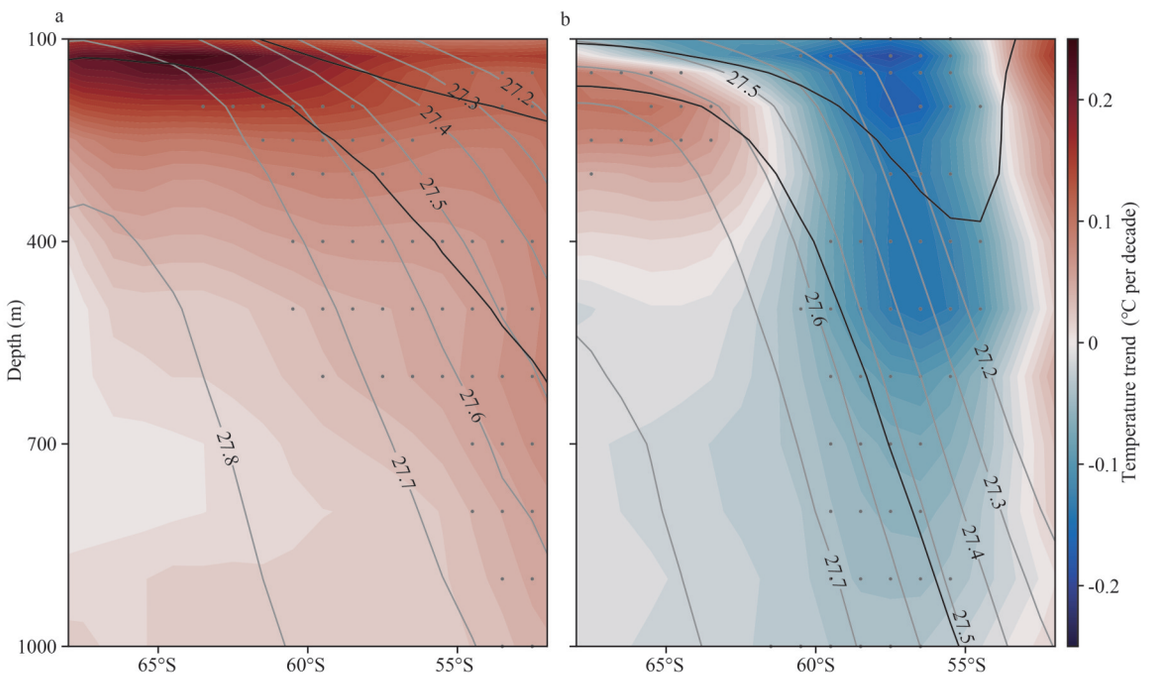

Fig.3 Zonal mean temperature trend during 1979–2019 based on Ishii

a. Ind sector; b. Pac sector. Solid lines from the surface to the deep indicate isohalines of 34.2 and 34.5, respectively. Gray lines denote the isopycnal with the 0.1-kg/m^3 interval.

cold tongue extending deep into the intermediate ocean. The cold tongue is associated with the transport of water mass (Carter et al., 2008). Additionally, we also notice that there is little difference between AAIW in the neutral density range and AAIW in the potential density range. The differences in the depths of AAIW less than 20 m have little effect on the average temperature and changes in heat content of AAIW.

We further find that there is also a zonal asymmetry in temperature and salinity changes of AAIW between Indian and southwest Pacific sectors in vertical (Fig.4). Temperature and salinity change in density coordinate rather than the depth coordinate is presented to show the properties changes of water mass in detail. Warming is occupied in the Indian sector (Fig.4a–c), with the most significant warming in the southeast Indian sector and reaching 0.14 °C per decade in 27.5 kg/m^3 after 1979. AAIW in the Atlantic sector also shows a warming, although it is partially offset by surface cooling. In contrast, cooling is robust in the South Pacific sector, especially in the southwest Pacific sector from 27.2 to 27.5 kg/m^3. The strongest cooling trend is more than -0.14 °C per decade in 27.5 kg/m^3 (Fig.4c). When it comes to the temperature/salinity trend in density coordinate, the zonal asymmetry of temperature and salinity changes of AAIW are also significant. Indian AAIW exhibits a warming trend of 0.05 °C per decade in 27.5 kg/m^3 and a salting trend of 0.005 per decade in 27.5 kg/m^3 (Fig.4d, significant at the 95% level). Compared with the mildly warming surface water, the subsurface water is relatively warmer. While southwest Pacific AAIW shows a cooling trend of -0.05 °C per decade in 27.3 kg/m^3 and a freshening trend of 0.004 per decade in 27.3 kg/m^3.

The thickness and depths of AAIW also play an important role in affecting its heat content changes. Previous studies suggest that changes in thickness dominate heat content, for example, the thickening of Subantarctic Mode Water accounted for more than 70% of the increase in heat content (Gao et al., 2018). Our study further finds that the increase in heat content lags the increase in thickness by approximately 5 months. This result indicates that the significant and continuous thickening can cause a persistent increase in heat content, and the response of changes in heat content occurs after five months rather than real-time response. The heat content and thickness of AAIW show a positive correlation, and their correlation coefficient reaches 0.81 (Fig.5a), as the thicker water mass has a greater capacity for heat storage and its temperature is increasing. Figure 5a displays the thickness trends in the two sectors. Indian AAIW thickened by 0.1 m

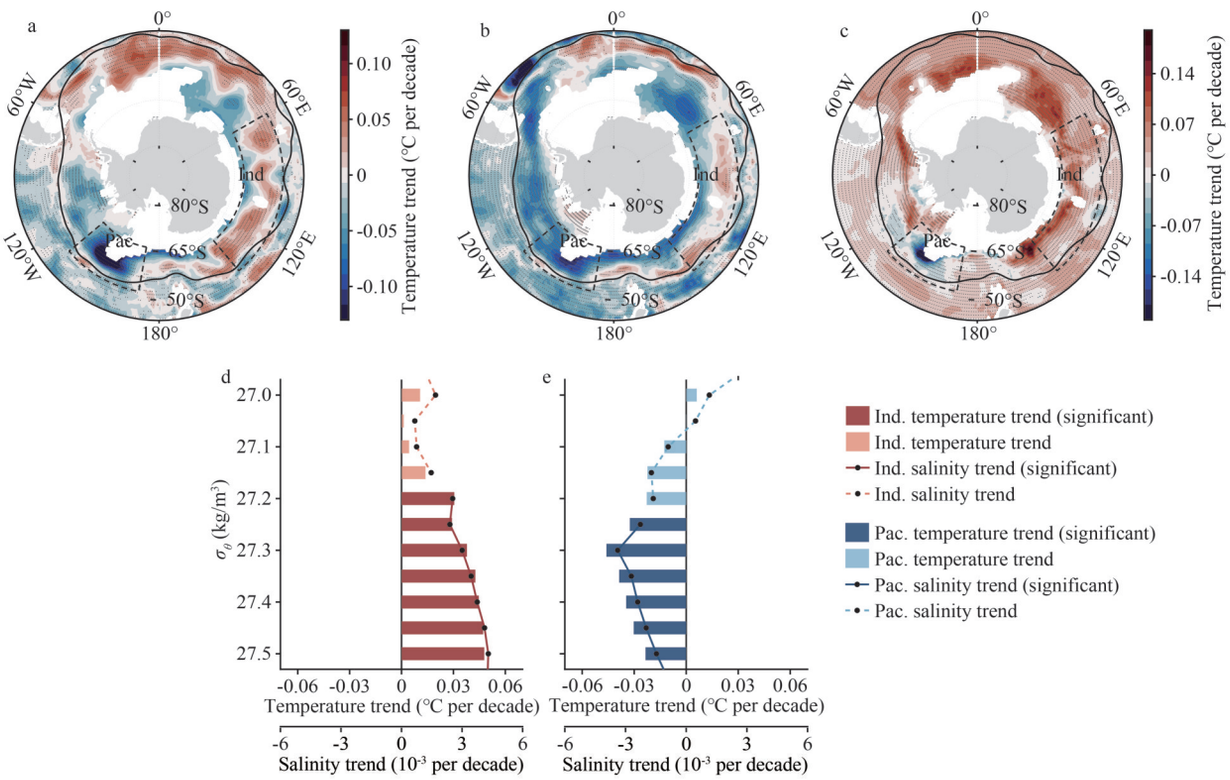

Fig.4 Temperature and salinity change of AAIW

a. average temperature trend of AAIW (27.2–27.5 kg/m^3); b and c. same as (a) but for upper layer of AAIW (27.2 kg/m^3) and lower layer of AAIW (27.5 kg/m^3), respectively; d. temperature/salinity trends under the density coordinate from to 27.5 kg/m^3 in the Indian sector with an interval of 0.05 kg/m^3. Dark color bar shows the significant temperature trends, and solid line shows the significant salinity trends (Alpha=0.05). Dashed line and light color bar denote the trends of temperature and salinity fail to pass the exceeding the 95% confidence level. Temperature trend uses the *x*-axis (unit: °C per decade) and salinity trend uses the *x*-axis (unit: 10^{-3} per decade).

per decade with a steady warming trend reaching 0.03 °C per decade during the same time. The upper and lower layers of the Indian AAIW deepen by 3.3 m per decade and 3.4 m per decade, respectively (Fig.5b). The lower layer deepens more significantly than the upper layers. In other words, the thickness of these two layers has increased, and the Indian AAIW is thickening. Thus, the thicker AAIW gains more heat, occurring in the intermediate ocean, and then the heat content of AAIW increases, whereas Indian AAIW is thinning during 2005–2019 with warming and an increase of heat content at the same time. That is, the increase of heat content in the Indian AAIW is associated with temperature after 2005. At the same time, the southwest Pacific AAIW is thinning by -1.7 m per decade and cooling by -0.06 °C per decade (Fig.5c), a thinner water mass contains less heat, and the temperature and heat content of AAIW decrease. This thinning of the southwest Pacific AAIW results from the stronger shallowing of the lower layers than that of the upper layer. The shallowing trend of the lower (upper) layer was -2.1 m (-0.3 m) per decade (Fig.5d). However, in the south of the SAF, the depth changes of AAIW in the Indian (southwest Pacific) sector only accounts for 18.3% (10.1%) of the thickness change though the depth change of the AAIW is consistent with the trend of heat content. Therefore, the impact of temperature change on heat content cannot be ignored.

The temperature and salinity changes mentioned above are closely related to the heat redistribution of water mass, and heat convergence and/or divergence and so on (Gao et al., 2018; Carter et al., 2022). For example, warming in the south Indian Ocean is associated with the heat convergence driven by the enhanced westerly wind (Yang et al., 2020). In the view of tilting isopycnals in the Southern Ocean and the AAIW from the surface to the intermediate ocean, its movement and property changes are closely related to the negative anomaly of wind stress curl, which shallows the surface layer via upward Ekman pumping and also induces the surface heat divergence (Wang et al., 2021; Song

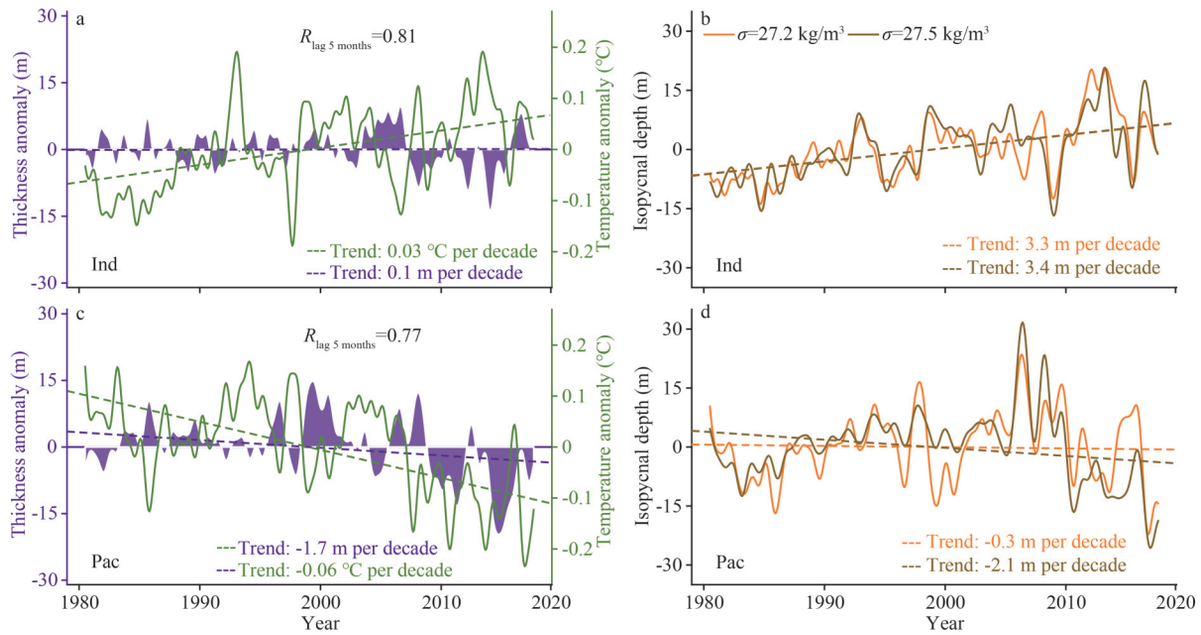

Fig.5 Temperature, thickness, and depth changes of AAIW

a. changes of temperature and thickness of the Indian AAIW. Purple shadow and green line denote thickness (right *y*-axis) and temperature (left *y*-axis) changes, respectively; *R* denotes the correlation coefficient between heat content and thickness of AAIW; b. depth changes of upper (27.2 kg/m^3) and lower layer (27.5 kg/m^3) AAIW in the Indian sector. The orange and brown lines represent depths of 27.2 and 27.5 kg/m^3, respectively; c. same as (a); d. same as (b), but for the southwest Pacific AAIW.

et al., 2024). On the other hand, the temperature and depths of AAIW show a significant variation beyond the seasonal timescale, especially on the annual to interannual timescale, superimposed on long-term trends (Fig.5). Given that the change of wind fields is related to the variation of large-scale circulation by the influence of climate variability (see more details in Section 4), we give the recent changes in the climate variability index of large-scale circulation.

Figure 6 displays the recent changes of interannual and decadal climate variability in the Southern Ocean over the past 40 years. The correlation coefficients between these indices and the heat content of AAIW in each sector are shown in Table 2 (at 95% significance level). SAM has exhibited a persistent positive trend since 1979. Its frequent positive phase has also been reported by many previous studies (e.g., Marshall et al., 2013). Although SAM has a circumpolar zonal wind in the Southern Ocean, it shows good correlation with the heat content changes in the Indian sector (R=0.56) during 1979–2019 but had little impact on the Pacific sector ($|R|$<0.2) (not shown). SAM has a longer-term influence compared to IOD since R= 0.56 is significant during 1979–2019. We checked the wavelet analysis of SAM and IOD and found that SAM had a longer signal of significant 64-

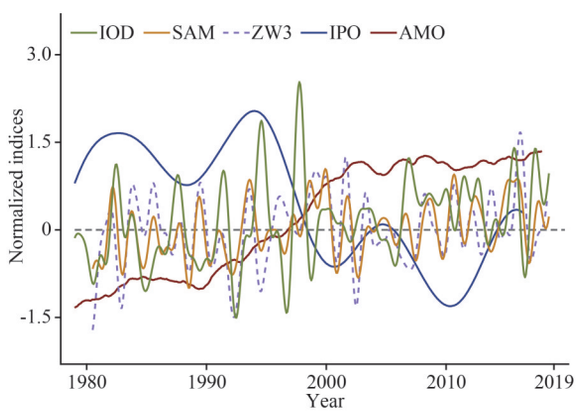

Fig.6 Indices of climatic variability during 1979–2019

Green line, orange line, purple dashed line, blue line, and red line denote IOD (Saji and Yamagata, 2003), SAM (Marshall, 2003), ZW3 (Raphael, 2004), IPO, and AMO index, respectively. The IPO index is filtered by 131 months (Henley et al., 2015), and the AMO index is smoothed by 121 months and detrended (Enfield et al., 2001).

month signal, but IOD had only 32 months. IOD has an important impact on sea ice change. After 2005, IOD usually expresses a positive phase, and exhibits a positive correlation with heat content changes in AAIW, and the coefficient changed from -0.36 during 1979–1993 to 0.51 during 2005–2019. The ZW3 (Zonal Wave Three) influences seasonal to interannual changes, but its influence is concentrated on the southwest Pacific sector (Jena et al., 2022). The positive ZW3 events also occurred more

Table 2 Correlation coefficient between atmospheric circulations and heat content of AAIW in each sector

	Indian sector			Southwest Pacific sector		
	1979–2019	1979–1993	2005–2019	1979–2019	1979–1993	2005–2019
IOD	/	-0.36	0.51	/	/	/
SAM	0.56	/	/	/	/	/
ZW3	/	/	/	-0.38	-0.54	-0.44
IPO	/	/	/	0.52	-0.46	0.56
AMO	/	/	/	/	-0.43	-0.23

/ indicates that the correlation coefficient is not significant (α=0.05).

frequently after 2005, and its negative events had a reduction. The coefficients between ZW3 and heat content reached -0.44 after 2005 and -0.54 before 1993.

The IPO and AMO have primarily manifested as phase shifts during 1979–2019, which affect the low-pressure system and sea ice in the Pacific sector as mentioned by Li et al. (2015). The IPO (AMO) shifted from a significant negative (positive) phase before 1993 to a significant positive phase after 2005 (significance for change of more than 1.5 standard deviations). The IPO and AMO also show good correlation with heat content changes in the Pacific sector, but those correlations are not satisfactory in the Indian sector. The IPO shows a significant decreasing trend since the 1990s and expresses a negative correlation with heat content of southwest Pacific AAIW during 1979–2019 (R= 0.52) and 2005–2019 (R=0.56). After 2005, the IPO shifts to a negative phase and exhibits a significant decrease in heat content that occurred simultaneously (Fig.2c–e). The AMO also showed a significant positive trend after 2005, as mentioned in Chung et al. (2022). The correlation coefficient between AMO and heat content of southwest Pacific AAIW reaches -0.43 before 1993. After 2005, this correlation coefficient reduces to -0.23. After 2005, the impact of IPO on the cooling of Pacific AAIW may have increased, while the impact of AMO may have decreased partly. In this study, the temperature change includes the impacts of the IPO and AMO during 20 years before and 20 years after their transition. Therefore, the results can still explain the decadal influence of the transition of IPO and AMO.

However, the change in heat content of AAIW results from the influence of wind field modulated by multiple large-scale circulations, though the correlation coefficients provide an initial indication of the potential link between climate variability and heat content changes of AAIW. Therefore, the following analysis gives the changes of wind fields and sea ice during different influences of climate variability to explore and explain the mechanisms of AAIW heat content change.

4 INFLUENCE OF LARGE-SCALE CIRCULATION

4.1 Interannual impact

The variations of sea ice and winds are important influences associated with large-scale circulations. Sea ice and its melting water have a vital impact on the sea surface temperature. The composition analysis is employed, using the months with significant climate variability (more than 1.5 standard deviations). The spatial variation of the wind field and sea ice due to the enhancement of large-scale circulations can be highlighted by the difference between different phases. Figure 7 shows the changes in sea ice concentration and wind field between the positive phase and negative phase of large-scale circulations. The decrease of SIC facilitates warming by weakening the surface cooling in the Indian sector. SIC exhibits a widespread reduction except for a slight increase only around the southwest Indian sector during positive phases of IOD and SAM (Fig.7a–b). The maximum decrease of SIC reached 12.2%. Decreased SIC also allows an increase in the heat flux into the surface ocean. The heat flux gains 25.8 TW (1 TW=10^{12} W) during the positive IOD events relative to the negative IOD. The cooling influence is mostly offset by the significant decrease of sea ice in the Indian ocean sector although there is a weak increase of SIC during positive ZW3 (Fig.7c). It is important that the positive SAM brings about strong zonal wind and negative wind stress curl, leading to an upward Ekman pumping and thereby promoting the upwelling of relatively warm subsurface water, and resulting in warming of AAIW.

In contrast, in the southwest Pacific sector, sea ice increases significantly almost everywhere, with southwest wind prevailing during positive ZW3 compared to negative ZW3 (Fig.7c). Raphael (2007) proposed that ZW3 positive events enhance the cold air northward from the polar ocean. The present study finds that cooling results from the significant increase of SIC during positive ZW3. The northward cold air flow from the polar causes a decrease in sea surface temperature, and the maximum increase in SIC was 16.6% (Fig.7c). This

significant increase in sea ice offsets the decrease caused by positive IOD and SAM (Fig.7a–b). At the same time, there is a significant negative anomaly of wind stress curl, leading to a shallowing of isopycnal (Fig.8b) through inducing an upward Ekman pumping (Fig.7f). The shallowing of the

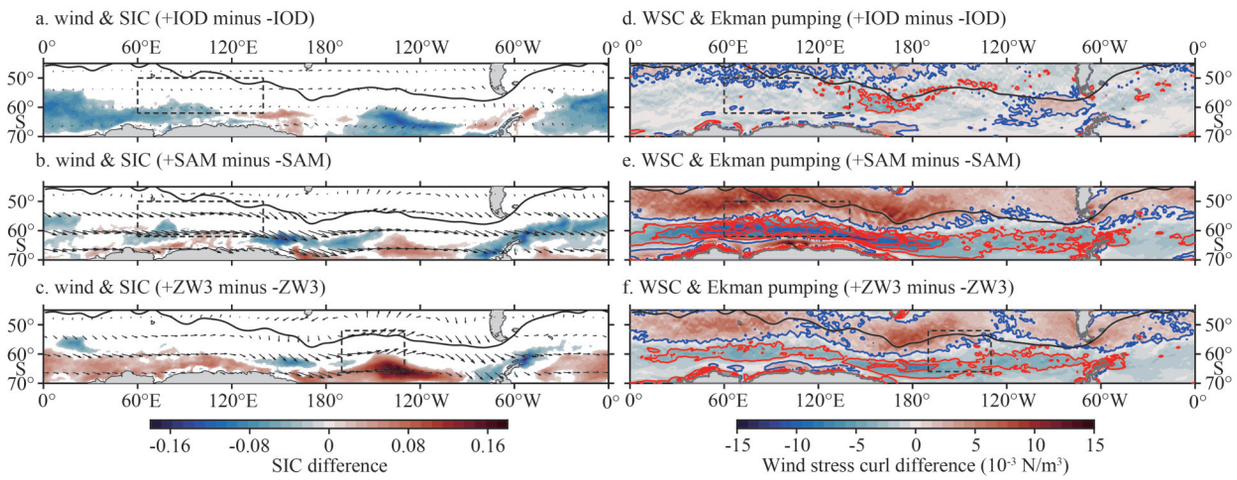

Fig.7 Change of sea ice and wind field

a. sea ice and wind field difference in the Indian sector between positive and negative IOD; b–c. same as (a) but for SAM (b) in the Indian sector and ZW3 in the southwest Pacific sector (c); d–f. same as (a–c) but show the wind stress curl and Ekman pumping difference. The red (blue) contour denotes upward (downward) Ekman pumping. Dashed black frames present the regions same as Fig.2a–d.

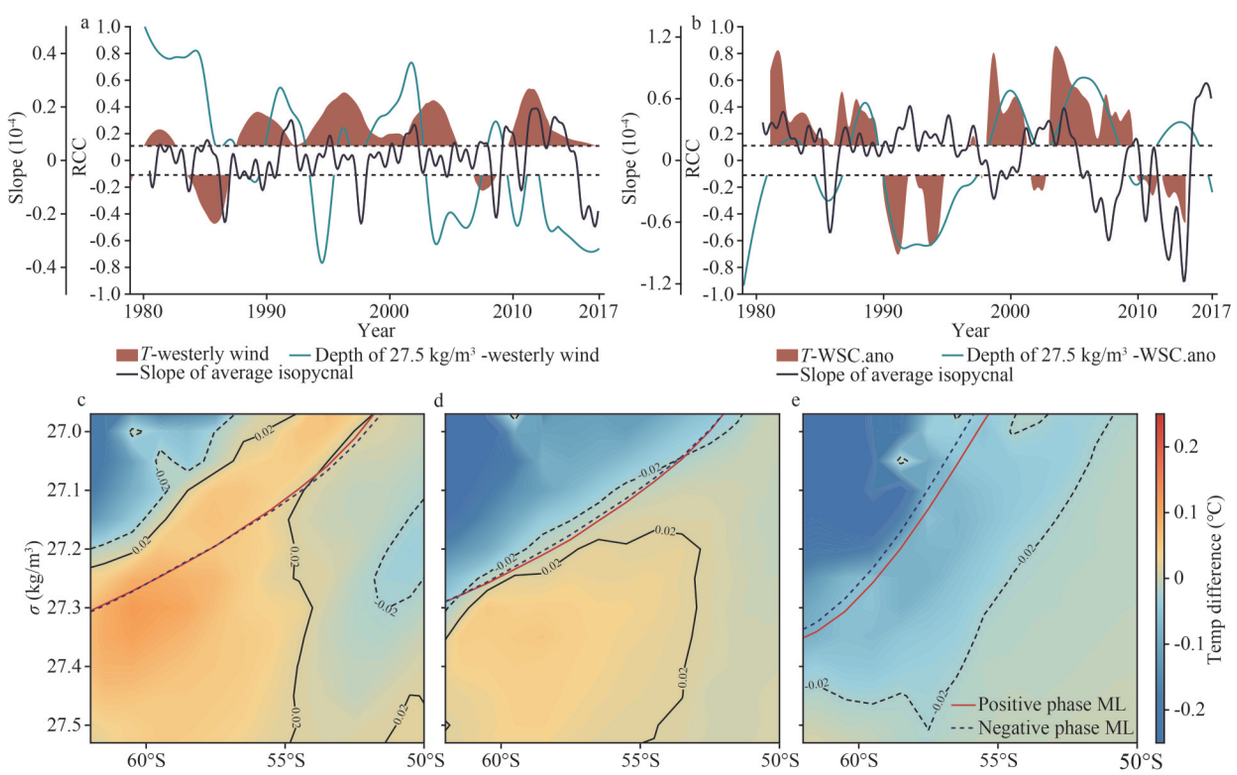

Fig.8 Running correlation coefficients (RCC) and slope of isopycnal

a. RCC in the Indian sector. Red shadow denotes (cyan line) the RCC between westerly wind and the mean temperature of AAIW (depth of 27.5-kg/m^3 isopycnal); b. RCC the southwest Pacific sector. Red shadow denotes (cyan line) the RCC between anomaly of wind stress curl (WSC.ano) and mean temperature of AAIW (depth of 27.5-kg/m^3 isopycnal). The blanks are the not significant coefficients (Alpha=0.05). The black line denotes the slope of the average isopycnal. The slope is derived by taking the difference in regional mean depth of the 27.5-kg/m^3 isopycnal between the north and south sides in each sector, divided by their meridional distance; c. temperature change in the Indian sector in the density coordinate between positive and negative IOD. The red solid line and the blue dashed line denote the mixed layer during the positive phase and negative phase, respectively; d–e. same as (c) but for SAM in the Indian sector and ZW3 in the southwest Pacific sector.

surface isopycnal in the south of 55°S leads to an increased tilt of the isopycnal (Fig.8b), which facilitates the sufficient cold surface water from the polar ocean to generate a cold AAIW. Li et al. (2022) explained the formation of AAIW by cold water from the polar ocean from the perspective of the water mass transformation. Then our study further reveals that this increase of the cold water from the polar ocean is caused by the intensified low pressure and sea ice due to the influence of the positive ZW3 events.

Moreover, although both the Indian Ocean sector and the Pacific sector are affected by the negative anomaly of wind stress curl, the change in heat content of AAIW is opposite. In the Indian sector, the negative anomaly of wind stress curl covers more than half of the ocean surface (Fig.7e), resulting in a general upwelling of subsurface warm water. On the other hand, the significant westerly wind anomaly is widespread (Fig.7b). The surface cold water is transported northward continuously due to the Ekman transport, and cooling is confined to the thin surface layer here (Haumann et al., 2020). Therefore, warming is significant in the Indian sector. In contrast, the negative anomaly of wind stress curl is only significant in the south of the Pacific sector (Fig.7f). This leads to the shallowing of the isopycnal occurring in the south, thereby causing the tilting of the isopycnal and promoting the cooling along the isopycnal (Fig.8).

Then, we explain the enhancement of the zonal asymmetry after 2005. Figure 8 gives a detailed description of the specific processes. The zonal asymmetry of AAIW heat content on an interannual time scale is attributed to the changes in sea ice and wind field (Fig.8). The running correlation coefficients (RCC) between westerly wind, wind stress curl, temperature of AAIW, and the depth of 27.5 kg/m^3 are given in Fig.8. The time series for running correlation are filtered over 16 months to analyze interannual changes. Changes of RCC reflect the influence of the wind field after 2005, which causes an enhancement of the zonal asymmetry of heat content trend in AAIW. The positive value of RCC indicates that when the westerly winds strengthen (the negative anomaly wind stress curl intensifies), deepening (shallowing) of isopycnal and warming (cooling) of AAIW occur, and vice versa. Additionally, the changes in the slope of the isopycnal are also presented. The slope is calculated as the ratio of the regional mean depth of AAIW to the zonal distance of each sector. Negative anomaly indicates an intensified south-to-north tilting of the isopycnal surfaces.

In the Indian sector, the westerly wind shows a positive correlation with the temperature of AAIW, and this positive correlation strengthens after 2005 (Fig.8a). That is, the warming of AAIW is influenced by the intensified westerly winds. Specifically, when the westerly wind strengthens, the northward Ekman transport also increases (Haumann et al., 2020), promoting the upwelling of subsurface warm water due to the continuity of water masses (Fig.8c–d). This upwelling is also promoted by the intensified upward Ekman pumping (Fig.7e). Here, the upward Ekman pumping primarily occurs in the south of 55°S, where the negative anomaly of wind stress curl is significant. However, there is a positive anomaly of wind stress curl and a downward Ekman pumping in the north of 55°S (Fig.8e), where the AAIW deepens and is thicker than that in the south. As a result, isopycnal of AAIW shows an overall deepening trend (Fig.5b). Furthermore, we also notice that the positive correlation between the AAIW temperature and the westerly wind is also strong before 2000, indicating that the influence of the westerly wind via the isopycnal is long-term and continuous (Fig.8a), whereas the influence associated with isopycnal usually needs a long time to affect ocean. Therefore, the warming of the Indian sector caused by the westerly wind became significant until 2005. In the southwest Pacific sector, the positive correlation between wind stress curl and AAIW temperature has strengthened since 2005. That is, the upward Ekman pumping increases (Fig.7f) affected by the negative anomaly of wind stress curl, leading to a tilting of the isopycnal (Fig.8b) and shallowing the depth of isopycnals in the south of 55°S (Fig.5d), which intensifies the tilt of the isopycnal surfaces (Fig.8b). Therefore, as sea ice concentration increases, sufficient surface cold water from polar ocean is provided (Fig.8e), and then tilting isopycnal surfaces promotes the effective formation of cold AAIW.

4.2 Decadal impact

The study period from 1979 to 2019 includes the transition of IPO and AMO during the 1990s, thus, the temperature changes before 1993 and after 2005 show the influence of the transition. The difference of wind field and SIC before and after the transition of IPO and AMO is shown in Fig.9. The heat content of AAIW in the southwest Pacific exhibited

two distinct periods. A decrease in heat content is occupied and persistent with a significant negative anomaly (<-1 ZJ) when positive AMO and negative IPO are both significant consistently (Fig.9a). However, the positive anomalies of heat content occurred during negative AMO and simultaneous positive IPO before 1993. Additionally, heat content experienced an interim period from 1993 to 2005. On the other hand, low-pressure system intensifies in the southwest Pacific sector during negative IPO and positive AMO, increasing SIC (Fig.9b–c). The west branch of the low-pressure system is the westerly wind and southerly winds, which transport cold air from the Antarctic to the north, increasing the temperature difference between the surface temperature and the SST, and thereby enhancing ocean heat loss, as mentioned by Raphael (2007).

We find that the increase of SIC occurs, leading to a decrease in the mixed layer temperature. The increase in SIC makes less ocean surface exposed to the atmosphere, thereby reducing surface heat flux (more details see Section 4.3). In the meantime, sea ice melting water provides a sufficient cold water supply for the mixed layer. The negative correlation between low-pressure system and mixed layer temperature, is significant, reaching 0.80 after 2005 (Fig.8c). At the same time, the increase of sea ice and meltwater cause the deepening of the mixed layer via the gathering cold water, which is significant after 2005 and strong enough (Fig.9c) though the low pressure system always promotes the shallowing of the mixed layer through Ekman pumping on interannual time scale. Li and England (2020) also find that the mixed layer has deepened in the Pacific sector during the surface cooling. Therefore, the cooling of the surface ocean can penetrate deeper into the subsurface ocean (Fig.3b).

Changes of heat content in AAIW in the southwest Pacific sector are closely associated with warm and/or cold-water input from the mixed layer,

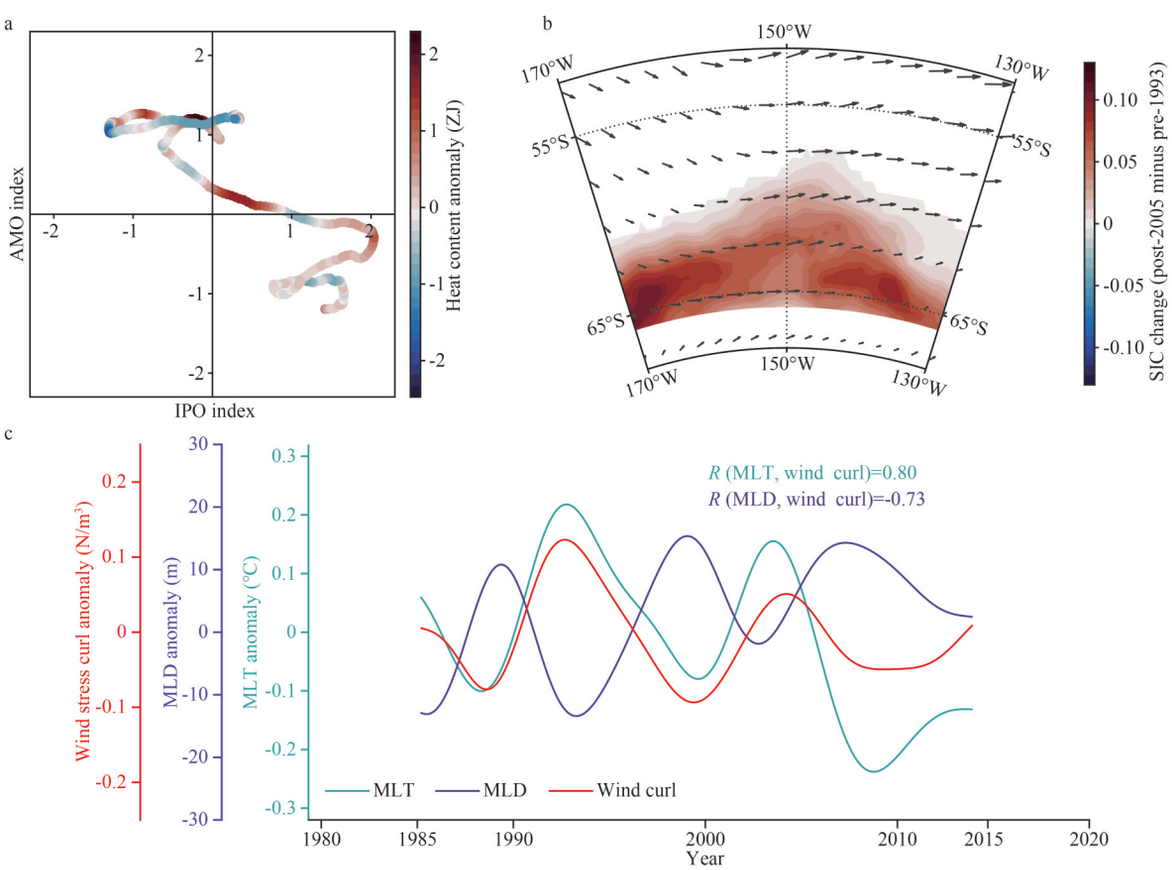

Fig.9 Heat content changes associated with sea ice, mixed layer temperature (MLT), mixed layer depth (MLD), and wind field curl

a. heat content anomaly of AAIW with AMO and IPO in the southwest Pacific sector; b. changes of SIC and wind between Period 1 and Period 2; c. changes of MLT (cyan line), MLD (purple line), and wind field curl (red line). The correlation coefficients are shown by the corresponding color. Time series are filtered by 36 months to analyze long-term changes.

which is significantly influenced by the wind anomaly. The wind curl anomaly is negative persistently after 2005, even though the amplitude of wind curl decreased (Fig.9c). Here, for an intuitive explanation of the negative wind stress curl, we define the half period of the time series as a full negative phase, which starts and ends at 0 value. For example, the wind stress anomaly from 1985 to 1990 has a half period of five years. The half period of wind curl changed from 1985–1990 to 2006–2013. The result reveals that the influence of the negative curl of wind stress has changed from lasting for 5 years to lasting for 7 years. The wind field anomaly changes to exist on a longer period than the interannual timescale and is influenced by the negative wind curl that exists persistently. Given the continuous influence of IPO and AMO on the mixed layer over a time scale of more than 10 years, the composition analysis of the mixed layer temperature and AAIW temperature lag the phases for 150 months. We find that the temperature anomaly of the mixed layer lags by 150 months after the significant phases of IPO and AMO, reflecting their delayed influence. And 150 months is enough for cold water across the mixed layer to cool the AAIW layer. Cooling of the mixed layer has obvious regional changes in neutral years when IPO and AMO were both weak. Warming occurs in the Indian sector and cooling occurs in the southwest Pacific sector but these trends are weaker than the most significant warming in the Atlantic sector (Fig.10a). However, when both positive AMO and negative IPO worked, cooling was widespread and significant in the Pacific sector (Fig.10b). This surface cooling penetrated to deeper layers and was facilitated by both positive AMO and negative IPO, which provided enhanced wind field with increasing sea ice. The process is that the stronger cyclonic anomaly (Fig.9b) shoals the mixed layer and subsequently the south part of the isopycnal is raised

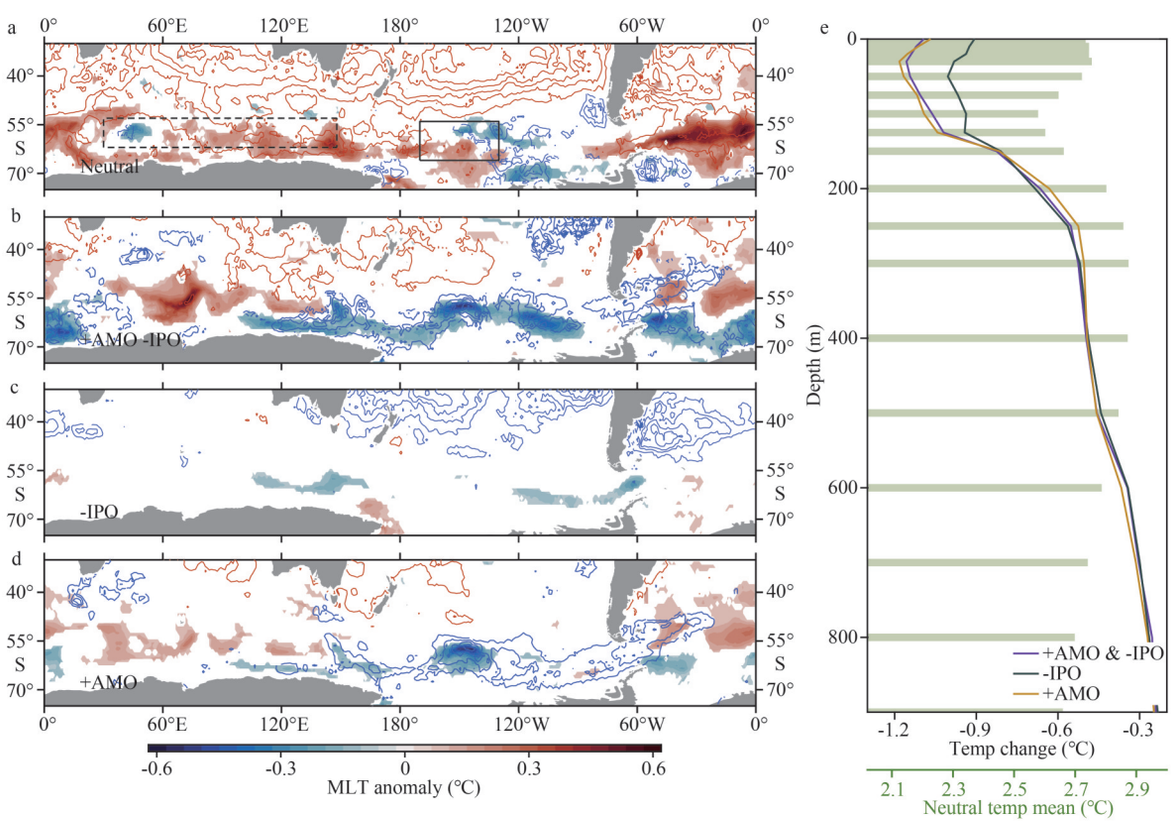

Fig.10 Compositions of MLT and AAIW temperature

a. MLT and AAIW temperature composition in the neutral year. Contours show the MLT anomaly with an interval of 0.1 °C. Shadow denotes AAIW temperature anomaly (show the values larger than a standard deviation, 0.08 °C); b–d. same as (a), but after 150 months after the positive AMO and negative IPO, negative IPO, and positive AMO, respectively; e. regional mean temperature profiles in the southwest Pacific sector. Light green bars denote temperature in the neutral year and use the light green *x*-axis at the bottom. Solid purple, dark green, and orange lines exhibit temperature in both positive AMO and negative IPO, negative IPO, positive AMO, respectively. Dashed (solid) black frames present the Indian (southwest Pacific) sector same as Fig.2a–d.

while the north part of the isopycnal changes little. Therefore, significant tilting of the isopycnal occurs (Fig.8b), and at the same time, enough cold water supplied by plentiful melting of sea ice intrudes into the deep along the tilted isopycnal. However, the temperature changes little when only negative IPO occurred (Fig.10c), and cooling is significant but limited in the southwest Pacific sector during positive AMO (Fig.10d). Cooling was significant within the mixed layer (<200 m) and reached deeper than 800 m when positive AMO worked (Fig.10e). Hence, cooling in the southwest Pacific sector is associated with mainly the positive shift of AMO and the negative shift of IPO. Additionally, both AMO and IPO start showing a significant positive correlation with the temperature of AAIW (R>0.5) when AMO and IPO lead the temperature 120 months, and the correlation coefficient gets larger with leading months. The impact of the transition of AMO and IPO on zonal asymmetry in the heat content trend of AAIW works on decadal or longer time scales (>12 years).

4.3 Contribution analysis

Based on the influence of large-scale circulations on the heat content changes of the AAIW sector through the wind stress curl and sea ice, it is necessary to clarify the combined effect of large-scale circulation. On the other hand, the relative importance of each large-scale circulation to heat content changes in the AAIW also needs analysis and quantification.

The combined effect of large-scale circulation dominates the zonal asymmetry in AAIW heat content change via the heat convergence/divergence induced by the wind field and sea ice. This influence of wind on temperature is closely related to the isopycnal (Ju et al., 2022). Here, we apply the heave-spice decomposition ($\frac{\mathrm{d}T}{\mathrm{d}t}\big|_{p} = \frac{\mathrm{d}T}{\mathrm{d}t}\big|_{\sigma} - \frac{\mathrm{d}p}{\mathrm{d}t}\big|_{\sigma}\frac{\partial T}{\partial p}$, Zunino et al., 2012) to explain the combined effect of large-scale circulation on the heat content change in the AAIW through the temperature variations related to isopycnal processes. Here σ represents the potential temperature. Heave $\left(-\frac{\mathrm{d}p}{\mathrm{d}t}\big|_{\sigma}\frac{\partial T}{\partial p}\right)$ shows the contribution due to vertical displacement of isopycnals on temperature, and Spiciness $\left(\frac{\mathrm{d}T}{\mathrm{d}t}\big|_{\sigma}\right)$ shows the contribution due to property change along isopycnal on temperature (Zunino et al., 2012). In the Indian sector, the negative anomaly of the wind stress curl (Figs.7–8) causes upwelling CDW accompanied by the relatively warm water transport along isopycnal. The heat convergence is mainly provided by the relatively warm CDW under 27.5 kg/m^3. Therefore, the wind stress curl results in the warming of 0.02 °C per decade in AAIW via the contribution of the heave and spiciness (Fig.11a). In the southwest Pacific sector, the increased sea ice melting is dominated in particular and provides the sufficient cold-water convergence via the spice, contributing to the cooling of -0.05 °C per decade in AAIW shown by the significant cold tongue, especially upon 600 m (Fig.11b). The contribution of the spiciness to the cooling is governed by the increased sea ice and its melting water.

Then, it is necessary to analyze the specific contributions of the combined effect of the large scale circulations. During 2015–2019, the heat content of AAIW in the Indian sector gained 0.9 ZJ as the equivalent of 336.0 TW total heat convergence. This warming is dominated by the upwelling CDW driven by the negative anomaly of the wind stress curl (Figs.7–8). The warming effect from heat flux (5.9 TW) is offset by the cooling effect from northward Ekman transport (-18.3 TW) driven by the westerly wind. In the southwest Pacific sector, the heat content of AAIW decreases by 0.4 ZJ as the equivalent of -149.3 TW heat divergence. This cooling is dominated by the sufficient cold water supplied by increased sea ice (Fig.7). Cooling due to the heat loss (-46.5 TW) is limited to the mixed layer <100 m, and the contribution of Ekman transport is relatively weak (-9.8 TW).

To further comprehend the relative importance of each large-scale circulation in each sector, we present the contribution of these atmospheric circulations on different time scales in Table 3. The contributions of IOD and SAM are the coefficients from the multiple linear regression of these two indices by the heat content of AAIW in the Indian sector. The contributions of ZW3, IPO, and AMO are the coefficients from the multiple linear regression of these three indices with the heat content of AAIW in the southwest Pacific sector. The contributions are the absolute values of their multiple linear regression coefficients. This contribution analysis gives the relative importance of large-scale circulation, considering the influence of co-factors. The increase of heat content of Indian AAIW is dominated by SAM and IOD on the

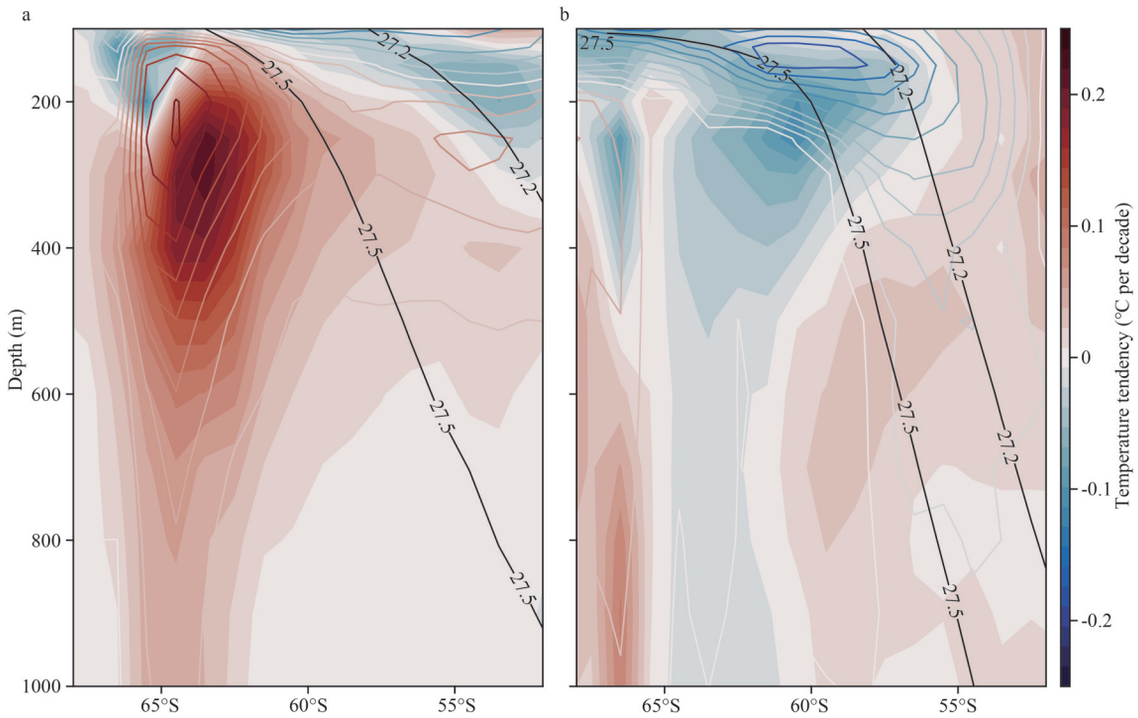

Fig.11 Contributions from heave (shadow) and spiciness (contours) to temperature variability in the Indian sector (a) and the southwest Pacific sector (b) during 2005–2019

All value is the average over each sector. The temperature variability has an interval of 0.02 °C per decade. Heave-Spiciness decomposition is referred to Zunino et al. (2012) and Ju et al. (2022).

interannual time scale (1–3 years). The warming contribution of SAM increases more than tenfold, and the warming influence of IOD increases sixfold after 2005. In the southwest Pacific sector, cooling is attributed to the transition of IPO and AMO on the decadal and/or long-time scale (>12 years), followed by the cooling influence of ZW3 on the interannual time scale. Above all, the positive phase of the AMO contributes nearly one-fifth of the decrease in the heat content of AAIW.

5 DISCUSSION AND SUMMARY

The Southern Ocean has been warming under rapid climate change. In this study, observational and objective analysis datasets are used to analyze the heat content changes of AAIW. This study reveals that the AAIW exhibits zonal asymmetry in heat content trend between the Indian sector and the southwest Pacific sector. AAIW in our study includes partly AASW. More importantly, our study finds that an unexpected zonal asymmetry existed in the intermediate ocean rather than limited to the surface layer. This heat content change in AAIW is non-negligible, as it affects the heat transport of ocean circulation and heat exchange between water masses. This zonal asymmetry is significant above 1 500 m, rather than confined to the surface, based on observation. The heat content of AAIW shows a significant increase by 0.4 ZJ per decade in the Indian sector, which is equivalent to a heat gain rate of 0.04 W/m^2 during 1979–2019 in the Southern Ocean between 40°S and 70°S. This heat gain rate

Table 3 Contribution of large-scale circulations to heat content changes of AAIW in each sector

Sector	Period	IOD[1]	SAM[1]	ZW3[2]	IPO[2]	AMO[2]
Indian sector	1979–1993	4.0%	1.6%			
	2005–2019	24.9%	13.1%			
Southwest Pacific sector	1979–1993			22.8%	4.7%	15.5%
	2005–2019			11.7%	4.7%	16.1%

1: used in the multiple linear regression in the Indian sector; 2: used in the multiple linear regression in the southwest Pacific sector.

can reach one-tenth of the 700-m heat content anomaly from 1993 through 2020 over the Earth's surface area, as reported by the State of the Climate 2020 (Blunden and Boyer, 2021). Heat content changes also show significant interannual to decadal variations superimposed on a long-term trend. The heat content of AAIW in the southwest Pacific sector has exhibited an unexpected decrease of -0.2 ZJ per decade since 1979, and this decreasing trend has intensified after 2005. Our study reveals that this cooling can offset nearly half of the heat gain, and this zonal asymmetry in the heat content of AAIW results from the different responses to the atmospheric circulations.

The opposite heat content changes in the Indian and Pacific sectors are contributed by the combined effect of large-scale circulations via the heat convergence/divergence, which is induced by the warm deep water upwelling and sea ice melting. Specifically, the interannual to decadal variations in the heat content of AAIW are caused by the atmospheric circulation. The warming of the Indian Ocean sector is dominated by heat convergence caused by the negative wind stress curl during positive SAM events. The combined effect of SAM and IOD causes the warming on the interannual time scale. The warming effect of SAM has been intensified since 2005 and is nearly ten times larger than that before 1993. Furthermore, the contribution of IOD to warming is partly offset by the cold water brought by the northward Ekman transport. Cooling in the southwest Pacific sector is dominated by the enhancement of the low-pressure anomaly. This combined effect of cooling is mainly caused by the transition of IPO and AMO on the decadal time scale, followed by the interannual impact from ZW3. The differences between the two decades and the lagging over ten years in the composition analysis reveal the influence of the transition of IPO and AMO, though the forty years are limited for analyzing the interdecadal impact of large-scale circulations. It should be noted that the positive phase of the AMO contributes nearly one-fifth of the decrease in heat content changes of AAIW on decadal and/or long-time scale (>12 years).

Additionally, in view of active eddy activities in the Southern Ocean, eddy heat transport is also important and requires eddy-permitting models and more accurate data assimilation methods in the future. In this study, the zonal asymmetry of heat content changes in AAIW between the Indian and southwest Pacific sectors may be enhanced with the continued positive AMO and negative IPO. Therefore, the south Indian may become the potential heat uptake pool of the Southern Ocean.

6 DATA AVAILABILITY STATEMENT

WOA 18 dataset and WOD 18 profiles are available and provided by the National Centers for Environmental information (NCEI) (https://www.nodc.noaa.gov/OC5/woa18/; https://www.ncei.noaa.gov/products/world-ocean-database). MOAA GPV observations is provided by JAMSTEC (https://www.jamstec.go.jp/e/). WOCE sections are free provided by CCHDO and are openly accessible online (https://cchdo.ucsd.edu/). The Ishii dataset is available at https://climate.mri-jma.go.jp/pub/ocean/ts/v7.3/. ERA5 dataset is available by ECMWF and the Copernicus Programme and the ERA5 dataset has been obtained in CDS (https://cds.climate.copernicus.eu). SAM index is accessed in https://www.bas.ac.uk/ and indices of IOD, IPO and AMO are available at https://psl.noaa.gov/.

7 ACKNOWLEDGMENT

The authors are grateful for the available ERA5 dataset provided conveniently by ECMWF and the Copernicus Programme. We also thank to the CSIRO Marine Research MATLAB Seawater Software Library.

Reference

Abernathey R P, Cerovecki I, Holland P R et al. 2016. Water-mass transformation by sea ice in the upper branch of the Southern Ocean overturning. *Nature Geoscience*, **9**(8): 596-601, https://doi.org/10.1038/ngeo2749.

Blunden J, Boyer T. 2021. State of the climate in 2020. *Bulletin of the American Meteorological Society*, **102**(8): S1-S475, https://doi.org/10.1175/2021BAMSStateoftheClimate.1.

Boyer T P, García H E, Locarnini R A et al. 2018. World Ocean Atlas 2018. NOAA National Centers for Environmental Information. https://www.ncei.noaa.gov/archive/accession/NCEI-WOA18. Accessed on 2024-11-12.

Carter L, Bostock-Lyman H, Bowen M. 2022. Water masses, circulation and change in the modern Southern Ocean. *In*: Florindo F, Siegert M, De Santis L et al. eds. Antarctic Climate Evolution. 2nd edn. Elsevier, Amsterdam. p.165-197, https://doi.org/10.1016/B978-0-12-819109-5.00003-7.

Carter L, McCave I N, Williams M J M. 2008. Circulation and water masses of the southern ocean: a review. *Developments in Earth and Environmental Sciences*, **8**: 85-114, https://doi.org/10.1016/S1571-9197(08)00004-9.

Cerovečki I, Meijers A J S, Mazloff M R et al. 2019. The

effects of enhanced sea ice export from the Ross Sea on recent cooling and freshening of the southeast Pacific. *Journal of Climate*, **32**(7): 2013-2035, https://doi.org/10.1175/JCLI-D-18-0205.1.

Chung E S, Kim S J, Timmermann A et al. 2022. Antarctic sea-ice expansion and Southern Ocean cooling linked to tropical variability. *Nature Climate Change*, **12**(5): 461-468, https://doi.org/10.1038/s41558-022-01339-z.

Clem K R, Lintner B R, Broccoli A J et al. 2019. Role of the south pacific convergence zone in west Antarctic decadal climate variability. *Geophysical Research Letters*, **46**(12): 6900-6909, https://doi.org/10.1029/2019GL082108.

Comiso J C, Nishio F. 2008. Trends in the sea ice cover using enhanced and compatible AMSR-E, SSM/I, and SMMR data. *Journal of Geophysical Research*: *Oceans*, **113**(C2): C02S07, https://doi.org/10.1029/2007JC004257.

Downes S M, Langlais C, Brook J P et al. 2017. Regional impacts of the westerly winds on Southern Ocean mode and intermediate water subduction. *Journal of Physical Oceanography*, **47**(10): 2521-2530, https://doi.org/10.1175/JPO-D-17-0106.1.

Dufour C O, Griffies S M, de Souza G F et al. 2015. Role of mesoscale eddies in cross-frontal transport of heat and biogeochemical tracers in the Southern Ocean. *Journal of Physical Oceanography*, **45**(12): 3057-3081, https://doi.org/10.1175/JPO-D-14-0240.1.

Enfield D B, Mestas-Nuñez A M, Trimble P J. 2001. The Atlantic Multidecadal Oscillation and its relation to rainfall and river flows in the continental U.S. *Geophysical Research Letters*, **28**(10): 2077-2080, https://doi.org/10.1029/2000GL012745.

Gao L B, Rintoul S R, Yu W D. 2018. Recent wind-driven change in Subantarctic Mode Water and its impact on ocean heat storage. *Nature Climate Change*, **8**(1): 58-63, https://doi.org/10.1038/s41558-017-0022-8.

Haumann F A, Gruber N, Münnich M. 2020. Sea-ice induced Southern Ocean subsurface warming and surface cooling in a warming climate. *AGU Advances*, **1**(2): e2019AV000132, https://doi.org/10.1029/2019AV000132.

Henley B J, Gergis J, Karoly D J et al. 2015. A tripole index for the interdecadal Pacific oscillation. *Climate Dynamics*, **45**(11): 3077-3090, https://doi.org/10.1007/s00382-015-2525-1. (Accessed on 28-03-2024)

Hersbach H, Bell B, Berrisford P et al. 2019a. ERA5 Monthly Averaged Data on Single Levels from 1940 to Present. Copernicus Climate Change Service (C3S) Climate Data Store (CDS). https://doi.org/10.24381/cds.f17050d7. (Accessed on 26-04-2022)

Hersbach H, Bell B, Berrisford P et al. 2019b. ERA5 Monthly Averaged Data on Pressure Levels from 1940 to Present. Copernicus Climate Change Service (C3S) Climate Data Store (CDS). https://doi.org/10.24381/cds.6860a573. (Accessed on 26-04-2022)

Hosoda S. 2007. Grid Point Value of the Monthly Objective Analysis Using the Argo Data. JAMSTEC, https://doi.org/10.17596/0000102. (Accessed on 22-11-2023)

Ishii M, Fukuda Y, Hirahara S et al. 2017. Accuracy of global upper ocean heat content estimation expected from present observational data sets. *SOLA*, **13**: 163-167, https://doi.org/10.2151/sola.2017-030.

Jena B, Bajish C C, Turner J et al. 2022. Record low sea ice extent in the Weddell Sea, Antarctica in April/May 2019 driven by intense and explosive polar cyclones. *npj Climate and Atmospheric Science*, **5**(1): 19, https://doi.org/10.1038/s41612-022-00243-9.

Jones M E, Bromwich D H, Nicolas J P et al. 2019. Sixty years of widespread warming in the southern middle and high latitudes (1957-2016). *Journal of Climate*, **32**(20): 6875-6898, https://doi.org/10.1175/JCLI-D-18-0565.1.

Ju W S, Zhang Y, Du Y. 2022. Subsurface cooling in the tropical pacific under a warming climate. *Journal of Geophysical Research*: *Oceans*, **127**(5): e2021JC018225, https://doi.org/10.1029/2021JC018225.

Kang S M, Yu Y, Deser C et al. 2023. Global impacts of recent Southern Ocean cooling. *Proceedings of the National Academy of Sciences of the United States of America*, **120**(30): e2300881120, https://doi.org/10.1073/pnas.2300881120.

Kolodziejczyk N, Llovel W, Portela E. 2019. Interannual variability of upper ocean water masses as inferred from Argo array. *Journal of Geophysical Research*: *Oceans*, **124**(8): 6067-6085, https://doi.org/10.1029/2018JC014866.

Li Q, England M H. 2020. Tropical Indo-Pacific teleconnections to Southern Ocean mixed layer variability. *Geophysical Research Letters*, **47**(15): e2020GL088466, https://doi.org/10.1029/2020GL088466.

Li X C, Gerber E P, Holland D M et al. 2015. A rossby wave bridge from the tropical Atlantic to west Antarctica. *Journal of Climate*, **28**(6): 2256-2273, https://doi.org/10.1175/JCLI-D-14-00450.1.

Li X, Cai W, Meehl G A et al. 2021. Tropical teleconnection impacts on Antarctic climate changes. *Earth & Environment*, **2**(10): 680-698, https://doi.org/10.1038/s43017-021-00204-5.

Li Z, Groeskamp S, Cerovečki I et al. 2022. The origin and fate of Antarctic intermediate water in the Southern Ocean. *Journal of Physical Oceanography*, **52**(11): 2873-2890, https://doi.org/10.1175/JPO-D-21-0221.1.

Liu W, Lu J, Xie S P et al. 2018. Southern ocean heat uptake, redistribution, and storage in a warming climate: the role of meridional overturning circulation. *Journal of Climate*, **31**(12): 4727-4743, https://doi.org/10.1175/JCLI-D-17-0761.1.

Locarnini R A, Mishonov A V, Baranova O K et al. 2019. World Ocean Atlas 2018 Volume 1: Temperature. NOAA, Silver Spring, MD, https://doi.org/10.25923/e5rn-9711.

Marshall G J, Orr A, Turner J. 2013. A predominant reversal in the relationship between the SAM and east Antarctic temperatures during the twenty-first century. *Journal of Climate*, **26**(14): 5196-5204, https://doi.org/10.1175/JCLI-D-12-00671.1.

Marshall G J. 2003. Trends in the southern annular mode from observations and reanalyses. *Journal of Climate*, **16**(24): 4134-4143, https://doi.org/10.1175/1520-0442

(2003)016<4134:TITSAM>2.0.CO;2.

McCartney M S. 1977. Subantarctic mode water. *In*: Angel M V ed. A Voyage of Discovery: George Deacon 70th Anniversary Volume (Supplement to Deep-Sea Research). Pergamon, Oxford. p.103-119.

Meijers A J S, Bindoff N L, Rintoul S R. 2011. Frontal movements and property fluxes: contributions to heat and freshwater trends in the Southern Ocean. *Journal of Geophysical Research*: *Oceans*, **116**(C8): C08024, https://doi.org/10.1029/2010JC006832.

Nuncio M, Yuan X J. 2015. The influence of the Indian Ocean dipole on Antarctic Sea ice. *Journal of Climate*, **28**(7): 2682-2690, https://doi.org/10.1175/JCLI-D-14-00390.1.

Portela E, Kolodziejczyk N, Maes C et al. 2020. Interior water-mass variability in the southern hemisphere oceans during the last decade. *Journal of Physical Oceanography*, **50**(2): 361-381, https://doi.org/10.1175/JPO-D-19-0128.1.

Raphael M N. 2004. A zonal wave 3 index for the Southern Hemisphere. *Geophysical Research Letters*, **31**(23): L23212, https://doi.org/10.1029/2004GL020365.

Raphael M N. 2007. The influence of atmospheric zonal wave three on Antarctic sea ice variability. *Journal of Geophysical Research*: *Atmospheres*, **112**(D12): D12112, https://doi.org/10.1029/2006JD007852.

Saji N H, Yamagata T. 2003. Possible impacts of Indian Ocean dipole mode events on global climate. *Climate Research*, **25**: 151-169, https://doi.org/10.3354/cr025151.

Sallée J. 2018. Southern Ocean Warming *Oceanography*. **31**(2): 52-62, https://www.jstor.org/stable/26542651.

Schmidtko S, JohnsonG C. 2012. Multidecadal warming and shoaling of antarctic intermediate water. *Journal of Climate*, **25**(1): 207-221, https://doi.org/10.1175/JCLI-D-11-00021.1.

Schmitz Jr W J, McCartney M S. 1993. On the North Atlantic circulation. *Reviews of Geophysics*, **31**(1): 29-49, https://doi.org/10.1029/92RG02583.

Song Y Y, Li Y L, Hu A X et al. 2024. Decadal thermal variability of the upper Southern Ocean: zonal asymmetry. *Journal of Climate*, **37**(11): 3117-3132, https://doi.org/10.1175/JCLI-D-23-0649.1.

Wang L N, Lyu K W, Zhuang W et al. 2021. Recent shift in the warming of the southern oceans modulated by decadal climate variability. *Geophysical Research Letters*, **48**(3): e2020GL090889, https://doi.org/10.1029/2020GL090889.

Yang L N, Murtugudde R, Zhou L et al. 2020. A potential link between the southern ocean warming and the South Indian Ocean heat balance. *Journal of Geophysical Research*: *Oceans*, **125**(12): e2020JC016132, https://doi.org/10.1029/2020JC016132.

Zhou J H, Li Y L, Du Y et al. 2024. Indian ocean intermediate water masses and their simulations by CMIP6 models. *Journal of Climate*, **37**(23): 6285-6303, https://doi.org/10.1175/JCLI-D-23-0667.1.

Zunino P, Schroeder K, Vargas-Yáñez M et al. 2012. Effects of the Western Mediterranean Transition on the resident water masses: pure warming, pure freshening and pure heaving. *Journal of Marine Systems*, **96-97**: 15-23, https://doi.org/10.1016/j.jmarsys.2012.01.011.

Zweng M M, Reagan J R, Seidov D et al. 2019. World Ocean Atlas 2018, Volume 2: Salinity. NOAA, Silver Spring, MD, https://doi.org/10.25923/9pgv-1224.